Mechanically Programmable Bend Radius for Fiber-Reinforced Soft Actuators

Kevin C. Galloway[1], Panagiotis Polygerinos[2], Conor J. Walsh[3], and Robert J. Wood[4]

Abstract— Established design and fabrication guidelines exist for achieving a variety of motions with soft actuators such as bending, contraction, extension, and twisting. These guidelines typically involve multi-step molding of composite materials (elastomers, paper, fiber, etc.) along with specially designed geometry. In this paper we present the design and fabrication of a robust, fiber-reinforced soft bending actuator where its bend radius and bending axis can be mechanically-programed with a flexible, selectively-placed conformal covering that acts to mechanically constrain motion. Several soft actuators were fabricated and their displacement and force capabilities were measured experimentally and compared to demonstrate the utility of this approach. Finally, a prototype two-digit end-effector was designed and programmed with the conformal covering to shape match a rectangular object. We demonstrated improved gripping force compared to a pure bending actuator. We envision this approach enabling rapid customization of soft actuator function for grasping applications where the geometry of the task is known a priori.

I. INTRODUCTION

The inherent compliance in soft material robotic systems enables capabilities and task versatility not found in traditional rigid-bodied robotic systems. For example, complex motions can be embedded into a monolithic structure, which reduces the mechanical complexity (i.e. no moving parts), manufacturing costs, and can simplify the controls overhead [1], [2], [3]. Soft systems also offer improved safety as these actuators (typically pneumatic or hydraulic) are inherently safe for interfacing with humans, animals or fragile objects due to their natural compliance and back drivability [4].

The soft material actuators found in these soft systems are typically constructed from a combination of elastomeric and inextensible but flexible (i.e. woven and non-woven) materials. Upon pressurization, embedded channels or chambers in the soft actuator expand in directions with the lowest stiffness and give rise to linear, bending, and twisting motions. For example, a McKibben actuator swells radially and contracts lengthwise upon pressurization to shorten the overall length [5]. A bending actuator - the focus of this work - combines a linear extending actuator with a strain limiting layer along the length. As the actuator is pressurized, part of it grows in length while the strain limited portion cannot, causing the actuator to bend.

This concept is well established and a variety of approaches have been demonstrated to achieve this function. For example, in 1967, James Baer patented a bellows-inspired soft actuator that could bend around an object in response to fluid pressure [6]. In another example, [7] presents a multi-degree of freedom bending actuator composed of three parallel chambers ($120°$ apart) contained in a fiber reinforced tubular elastic body. These works and many others [8], [9], [10], [11], [12], [13] present methods for creating bending soft actuators; however, no one has yet - to our knowledge - presented a method for rapidly programming the bend radius and bending axis of a soft bending actuator by modifying the mechanical structure. This has relevance towards improving the agility of soft actuators - the ability to create intricate movements - by enabling the user to adjust the placement and magnitude of a bending actuator's radius of curvature [2]. As a point of comparison, the rigid mechanical joints in a traditional robotic system enable precise and intricate motions; however, these systems typically have long engineering design cycles with expensive components (e.g. motors, bearings, etc.) and precision machined parts - all requiring time and expense to source, manufacture, assemble and ship. The materials in soft material robotics offers an alternative approach to the design cycle where it is possible to rapidly and inexpensively fabricate custom actuators on-site.

II. SOFT ACTUATOR FABRICATION

A. Fabrication of a Bending Soft Actuator

The fiber reinforced (FR) soft bending actuator (see Fig. 1 for cross-sectional views) used in this study is fabricated using a multi-step molding process. This approach offers complete control over every aspect of the assembled soft actuator including geometry, material properties, and fiber reinforcements. The molds for the actuator were 3D printed with an Objet Connex 500 (Fig. 2). The first rubber layer (labeled 'rubber' in Fig. 1 and pictured in Fig. 3a) has a 2mm wall thickness and used a 15.88 mm (0.625 inch) diameter half round steel rod to define the interior, hollow portion of the actuator. After molding the first rubber layer, fiber reinforcements were added to the surface (Figs. 3a-b). Woven fiberglass (S2-6522 plain weave 4 oz. weight) was glued to the flat face to serve as the strain limiting layer that promotes bending during fluid pressurization (Fig. 3a). A single Kevlar thread (0.38 mm diameter) was then hand wound around the length of the actuator body to constrain radial swelling during

[1]K. C. Galloway is a research engineer with the Wyss Institute at Harvard University, Cambridge, MA 02138 USA (kevin.galloway at wyss.harvard.edu).

[2]P. Polygerinos is a post-doctoral research fellow in the Wyss Institute and School of Engineering and Applied Science (SEAS) at Harvard University.

[3]C. Walsh is an assistant professor of Mechanical and Biomedical Engineering in the Wyss Institute and SEAS at Harvard Univesity.

[4]R.J. Wood is the Charles River Professor of Engineering and Applied Sciences in the Wyss Institute and SEAS at Harvard University.

pressurization (Fig. 3b). Raised features in the mold were transferred to the actuator surface and defined the thread path - 3mm pitch - for consistency of thread placement (Fig. 2). Fiber reinforcements were further secured by placing the entire assembly into another mold to encapsulate the actuator body in a 1 mm thick silicone layer (labeled 'FR rubber' in Fig. 1 and pictured in Fig. 3c). The actuator body was then removed from the mold and the half round steel rod. The first open end was capped by placing it into a small cup of uncured silicone. Once this end cured, a 10-32 vented screw was fed through the silicone cap and became the mechanical connection for the pneumatic tubes (see Fig. 3d). The other open end was capped in a similar manner. As a final assembly step, a single-barbed tube fitting was screwed into a 10-32 threaded female stand-off and this assembly was threaded onto the end of the vented screw (Fig. 3e). When a pressurized fluid is applied to the interior of this bending actuator, it produces the motion shown in Fig. 4.

Fig. 2. Image of one of two molds used in the soft actuator fabrication process. The steel half round defines the hollow interior portion of the actuator while the 3D printed mold defines the outer shape and includes raised features that define the thread placement for fiber reinforcement.
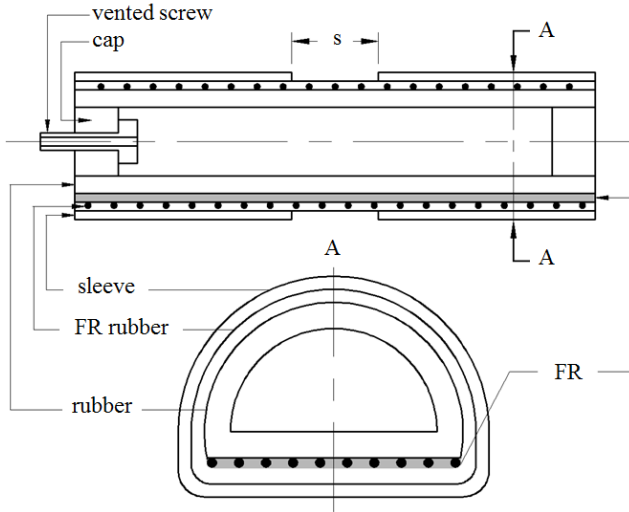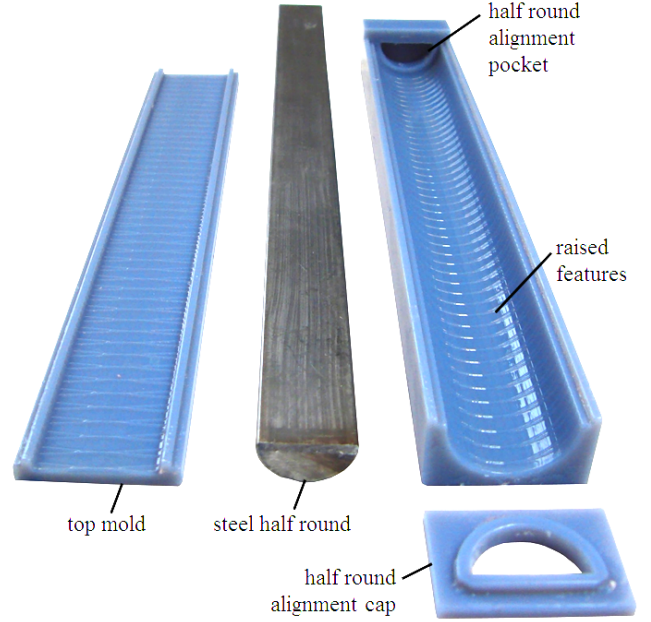

Fig. 1. Cross-sectional views of the fiber reinforced soft bending actuator. These features are not drawn to scale.

B. Using Sleeves to Mechanically Program a Bending Soft Actuator

The motion of a soft bending actuator can be altered with a form fitting covering - a sleeve - that acts as a strain limiting layer in all directions and significantly restricts covered portions from bending. The sections of the actuator that are not covered are free to bend. Adjusting the amount of free area between two sleeves (illustrated by the spacing, s, in Fig. 1) impacts the location and the magnitude of the actuator's bending radius of curvature. In practice, this is demonstrated in Fig. 5 with three different sleeve spacings: 0 (a single cut), 15 and 30 mm centered at the actuators midpoint. The sleeve material chosen for this work is Sure-Grip heat-shrink tubing, which is a polyolefin/polyester woven fabric that shrinks when heat is applied. Heat shrink tubing has many desirable properties including the ability to conform around irregular shapes, rapid installation (< 1 minute), simple alteration

(i.e. cut to length or cut holes to create free space), and reversibility as it can be removed with cutting tools.

The sleeves also offer a unique capability for interfacing rigid elements with a soft actuator. From a mechanical perspective, incorporating passive rigid elements into a soft actuator assembly has the advantages of constraining radial expansion on the flat surface and further stiffening actuator sections where bending is not desired. Fig. 6 illustrates this concept where Fig. 6a-b, depicts the bowing of the actuator's flat surface during pressurization with an illustrated cross section and actual side view. When FR laminate sheets (0.8 mm thick fiberglass laminate) are added and covered with a sleeve (Fig. 6c-d), the sleeve anchors the FR laminates, and the FR laminates reinforce the sleeved areas from bending (Fig. 7). This arrangement enables the actuator to achieve a smaller bending radius of curvatuve.

III. EXPERIMENTAL SET-UP

Using the fabrication process outlined in Section II, two 17 cm long soft bending actuators were created, one with a 10A durometer silicone rubber and the other with 28A (see Table I for comparison a material properties). These silicone rubbers where chosen for their extensibility and high tear strength properties.

A. Sleeve Attachment

All sleeves were attached in a two-step process. First, the actuator was inserted into the sleeve and a heat gun was used to tighten the sleeve around the actuator. Second, the sleeve spacing was created by drawing cut lines onto the sleeve with a marker and subtracting these areas. The cut
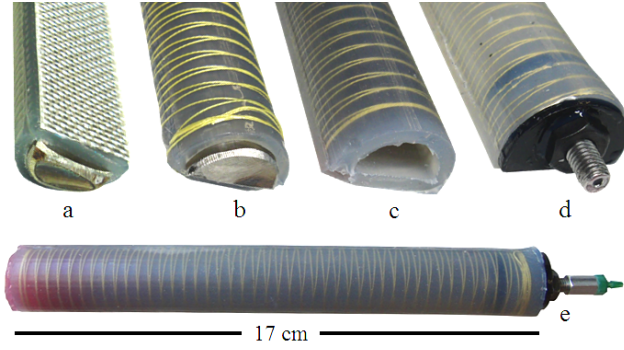
Fig. 3. Several stages of the soft actuator fabrication process. (a) After the first molding step shown in Figure 1, a strain limiting layer - woven fiberglass - is glued to the flat face. (b) Fiber reinforcing thread - Kevlar - is then hand wound along the entire length. (c) In the second molding step, the entire actuator is encapsulated in a 1mm thick layer of silicone to anchor all fiber reinforcements. (d) Both ends of the actuator are capped with one end supporting a vented screw. (e) Top view of the completed bending actuator with a barbed tube fitting threaded onto the vented screw. The entire assembly weighs less than 45 grams.

Fig. 4. Range of motion of the fiber reinforced soft bending actuator constructed from 28A durometer rubber (see Table I for material properties).

TABLE I

SUMMARY OF SILICONE MATERIAL PROPERTIES

Material	Shore A Hardness	Tensile Strength MPa (psi)	Elongation at Break %	Tear Strength N/mm (pli)
Dragon Skin 10*	10A	3.28 (475)	1000%	17.9 (102)
Elastosil M4601**	28A	6.5 (943)	700%	>30 (171)

*Smooth-On, Inc. (Easton, PA, USA)
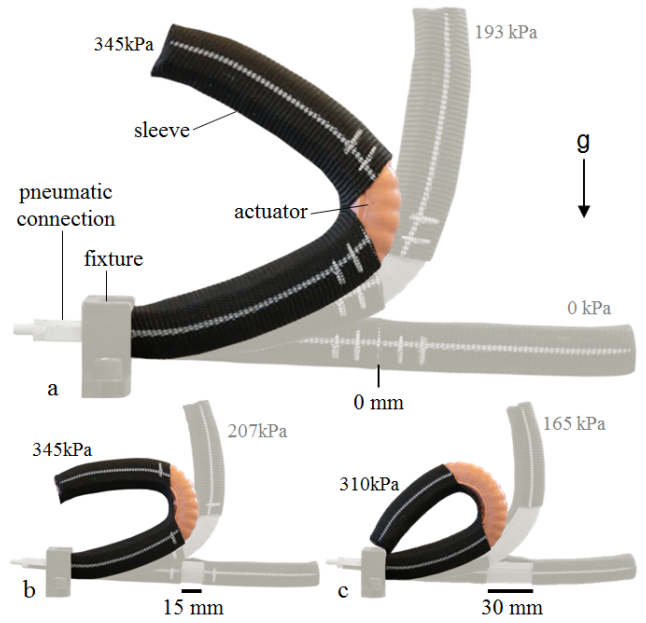**Wacker Chemical (Bankstown, AU)

Fig. 5. Range of motion comparison of a 28A durometer sleeved soft bending actuator at different sleeve spacings with (a) 0 mm, (b) 15 mm, and (c) 30 mm sleeve spacing. The shadow images show the actuators bending at different pressures.

lines were defined by a laser cut paper template that was wrapped around the actuator. Cutouts in the template enabled direct access to mark the sleeve surface, and scissors were used to remove the selected area. The sleeve material along the flat face of the actuator was not removed since this strain limited section of the actuator does expand lengthwise during actuation. This bridge material also ensures that sleeve spacing is maintained.

B. Evaluation Platform

An evaluation platform was developed to mechanically characterize the soft actuators. A data acquisition board (NI USB-6210, National Instruments) was used to measure and control all aspects of the system including an electronic pressure regulator (ER1, Wilkerson), solenoid valves (3-way, 2-position, X-Valve, Parker), pressure sensors, and flow sensors, and a thermistor for in-line air temperature monitoring. Additionally, two cameras are linked with the system: one monitors the platform (1080p HD webcam, Sony) while the other (Rebel T2i, DSLR, Canon) records images and videos for estimating the bending angle and radius of curvature. The recording camera is mounted on a tripod with a telephoto lens (EF 70-300 mm, Canon) that is fixed at 135 mm to minimize lens distortion effects and increase accuracy of measurements. For calibration and registration, a checkerboard printout was mounted directly behind and parallel to the actuator's plane of motion. Furthermore, a metric ruler was anchored to the actuators' fixture. This ruler provides a correlation between image pixels and actual length units. Lastly, the evaluation platform includes a six axis force/torque sensor (Nano17, ATI Industrial Automation)
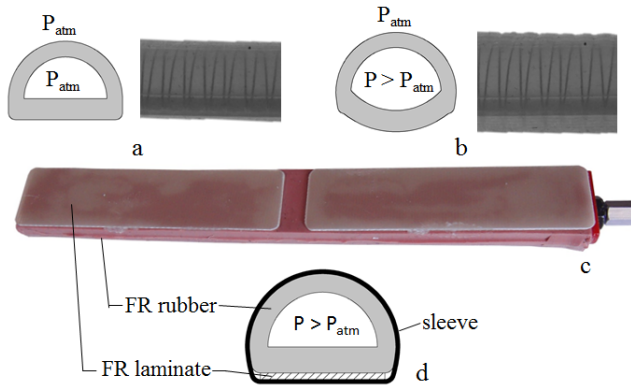
Fig. 6. Illustrated cross-section comparison of fiber reinforce actuator with and without fiber reinforced laminate where (a) shows an illustrated cross-section and actual side view of an unpressurized FR actuator, (b) shows expansion of the actuator walls due to fluid pressurization (note the outward bowing of flat face), (c) demonstrates placement of FR laminate on a FR actuator, and (d) shows an illustrated cross-section view of the actuator when a sleeve is added. The combination of the sleeve and FR laminate stiffen the flat face and eliminate visual indications of bowing.

which was used to measure the blocked force at the tip of the actuator when the actuator is pressurized from its neutral configuration.

C. Experimentation Protocol

For the experiments, three actuators were created; one with 10A and another with 28A durometer material. The third actuator, also constructed of 28A, encloses all FR laminates in the sleeved portions as depicted in Fig. 7, and will be referenced as 28A-FRL. All three actuators were tested at the three sleeve configurations: 0 mm (a single cut), 15 mm, 30 mm spacing.

Each actuator was cantilevered in the evaluation platform with one end - the pneumatic connection - anchored to a fixture (see Figs. 5 and 7). The unsupported actuator length was 16 cm (6.3 inches) for all cases. The 10A durometer actuator was pressurized up to 207 kPa (30 psi) while the 28A durometer actuators were pressurized up to 414 kPa (60 psi). During these experiments, the camera captured frames for post-analysis of the bending angle and radius of curvature. The frames analysis was done using video analyzer software (Dartfish 4.5). For each actuator, three fluid pressurization cycles were completed to increase accuracy of results and confirm repeatability. The frames were analyzed for the angle between the two sleeved portions, and the radius of curvature was measured at the maximum tested air pressure. For force measurement, a line level was used to bring the bottom surface of the actuator to the top surface of a rod attached to the force sensor. The rod tip was positioned at distal end of the actuator (see inset image in Fig. 9). The pressure was increased in 34.5 kPa (5 psi) increments and the resultant force was recorded.

IV. RESULTS AND DISCUSSION

The results of the soft actuator experiments reveal trade-offs in actuator performance between the sensitivity of angu-
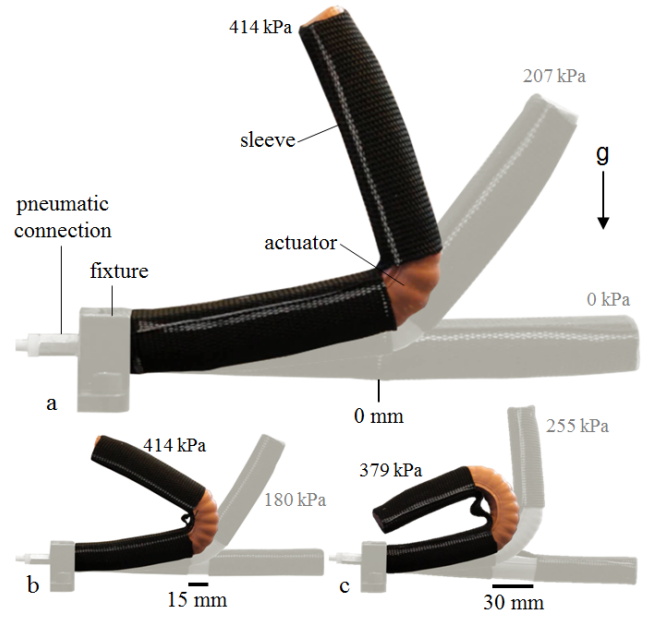

Fig. 7. Range of motion of a 28A durometer soft bending actuator with 0.8mm thick FR laminates on the flat surface with the (a) 0 mm, (b) 15 mm, and (c) 30 mm sleeve spacing. It should be observed that the actuator can achieve a smaller bending radius of curvature with the FR laminates than without (see Fig. 5).

lar deflection to fluid pressurization, output force, and radius of curvature.

With respect to angular deflection, the lower durometer rubber (10A) demonstrated the highest sensitivity to pressurization (see Fig. 8 and Table II for slope values). Sleeve spacing also affected sensitivity, where increased spacing correlated to increased deflection at a given pressure. This pattern appeared across all tested actuator types. As show in Table II, the slope from 0 mm to 30 mm configurations more than doubled for the 10A and 28A-FRL actuators, and increased 1.6x for the 28A actuator.
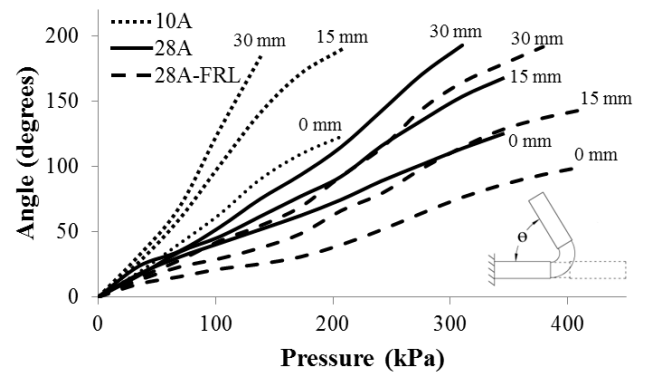

Fig. 8. Deflection angle between the two sleeved portions of the 10A, 28A, 28A-FRL actuators for a range of input pressures.

With respect to tip force measured from the neutral configuration, the higher durometer rubber was able to support higher pressures and thus produce larger output forces

ACTUATOR PERFORMANCE & LINEARITY

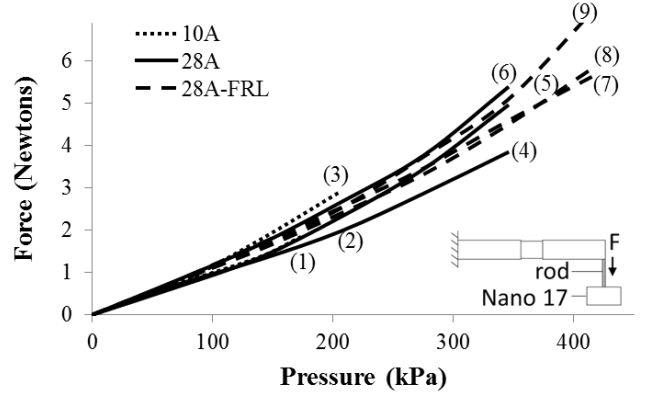| Actuator Type Identifier	Actuator Type	Sleeve Cut Size	Slope ($\Delta y/\Delta x$)	R^2
1	10A	0 mm	4.24	0.9948
2	10A	15 mm	6.59	0.9913
3	10A	30 mm	8.57	0.9743
4	28A	0 mm	2.53	0.9957
5	28A	15 mm	3.3	0.9953
6	28A	30 mm	4.07	0.9889
7	28A-FRL	0 mm	1.61	0.9762
8	28A-FRL	15 mm	2.4	0.9885
9	28A-FRL	30 mm	3.41	0.9808

Fig. 9. Force results for all actuator configurations. There is a similar output force response for these three different actuators. The only commonality between the actuators is the fiber reinforcement discussed in Section IIA. The number next to each curve corresponds to the 'Actuator Type Identifier' in Table II.
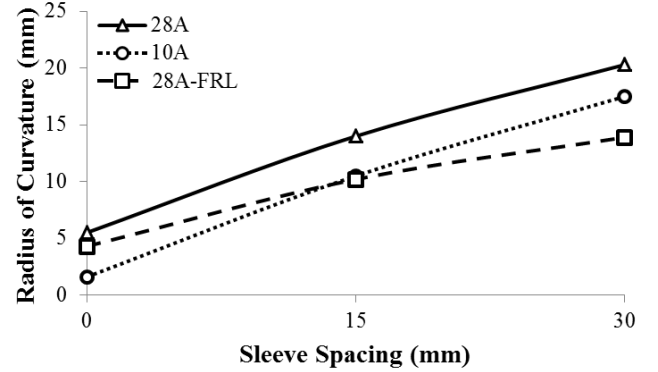

Fig. 10. Measured radius of curvature at maximum evaluated pressure.

(Fig. 9). For example, all sleeve configurations for the 28A-FRL actuator exceeded 5 N with the 30 mm configuration delivering the largest distal force of 7.12 N at 414 kPa (60 psi). In the 10A configuration, the 30 mm sleeve spacing produced the highest output force of 2.75 N at 172 kPa (25psi), and decreased marginally with the smaller sleeve spacings. It may be the case that the larger sleeve spacing correlates to more active actuator area and can contribute marginally more force. When the end-point force of all three actuators are evaluated together, they follow a similar trajectory (Fig. 9). The commonality among all three actuator configurations are the fiber reinforcements (i.e. woven fiberglass strain limiting layer and Kevlar thread winding) embedded in the actuator body (discussed in Section IIA). The close packing of the curves suggests that the fiber reinforcements play a larger role in the output force response of these actuators than material durometer (at least at low pressures). At high pressures, the 10A durometer actuator is unstable and prone to failure (e.g. they will easily fail at 400 kPa). Our experience suggests that while a lower durometer rubber may initially produce forces similar to a higher durometer rubber, the higher durometer rubber can support higher pressures and produce larger forces. This is a topic that deserves further investigation evaluating multiple FR configurations.

The radius of curvature measured at the maximum evaluated pressure increased as sleeve spacing increased (Fig. 10). Between the 10A and 28A durometer actuators, the 10A actuator is able to achieve a smaller radius of curvature for all sleeve spacing configurations. The 28A-FRL actuator showed the flattest response. At the zero mm sleeve position, the 28-FRL radius of curvature falls between the 10A and 28A; however, by the 30 mm sleeve spacing, this configuration achieved the lowest radius of curvature. This suggests that the FR laminates localize actuation to the sleeve spacing. Therefore, to achieve the tightest radius of curvature with a higher durometer rubber, a passive stiffening element such as FR laminate should be included.

V. CASE STUDY

The following case study evaluates the ability of two opposed 28A durometer actuators (Fig. 11) to shape match an angular object and achieve a significant payload holding capacity. The object is a rigid foam block (11 cm x 13 cm x 2.5 cm) and has a metal hook passing through which connects to a hanging bucket. The actuators were pressurized to 345 kPa (50 psi) and sand was gradually added to the bucket until the object dropped. Three actuator cases were tested including the standard sleeveless bending actuator, the zero mm sleeve spacing, and the FR laminate zero mm sleeve configuration. To minimize material friction comparisons, a small amount of sleeve material was bonded to the flat face of the rubber bending actuator to match the surface properties of the other cases. The ability of each actuator configuration to conform to the angular object is apparent in Fig. 11. The standard bending actuator (Fig. 11a) bows at the sides leaving considerable compliance for the actuators to deform with increasing payload. The zero mm sleeve configuration (Fig. 11b) bows much less at the sides and demonstrates improved comformability. The FR laminate and sleeve configuration demonstrates the best conformability

(Fig. 11c). In this preliminary study, the average payload capacity of the respective configurations is 3.45 kg, 4.68 kg, and 6.1 kg. This suggests that the proposed soft actuator sleeve method can be used to limit compliance of covered portions and increase payload holding capacity.
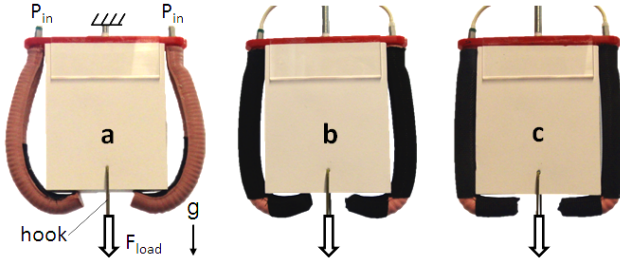

Fig. 11. The proposed sleeve method enables improved shape matching to angular objects and holding strength.

For the purpose of demonstration, Fig. 12 highlights the ability to rapidly alter the motion of a bending actuator by modifying the sleeve on-the-fly. In this example, a bending actuator was outfitted with three FR laminate segements. Fig. 12a shows the pressurized state without any spacings cut into the sleeve. Fig. 12b shows the same actuator with a single cut in the sleeve near the distal end. Fig. 12c shows the simplicity of adding a second joint and Fig. 12d demonstrates that sleeved portions can be cut away to recover bending motions. Figs. 12e-f further illustrate that the sleeve can be used to move the point where the actuator initially bends.
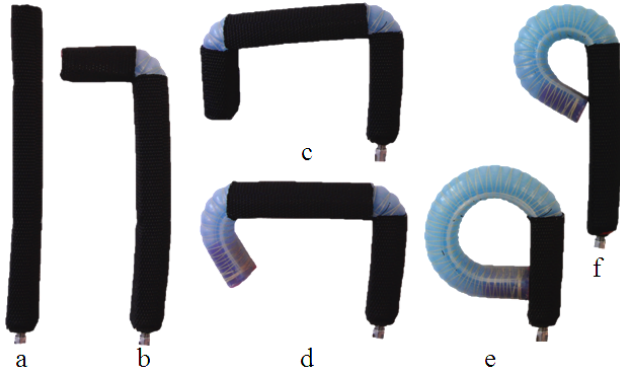

Fig. 12. A conformal sleeve applied to a bending actuator can be altered to generate a wide range of motions.

VI. FUTURE WORK AND CONCLUSIONS

We have focused on an empirical evaluation of using sleeves - a conformal covering - to rapidly and mechanically program motions into a soft bending actuator. The objective is to enable an end user to customize a soft actuator for a range of applications with these sleeves and circumvent the modeling, design, and manufacturing processes. In particular, we describe two techniques to rapidly change the bending behavior of an actuator to achieve joint-like motions: sleeves with and without FR laminates. Sleeve spacing and material durometer play a dominate role in deflection angle response to pressure where the lower durometer material and the larger sleeve spacing was most sensitive (i.e. deflected the most for the least amount of input pressure). The higher durometer materials were able to support higher pressures and thus generated larger forces; however, the relative similarity of the output force response at lower pressures suggests fiber reinforcements embedded in the actuator play a larger role than material durometer. We also found that for the higher durometer material, sleeves with FR laminates achieve the smallest radius of curvature for all tested sleeve spacings. Lastly, we demonstrated that for a known object geometry (i.e. angular geometry) sleeved and FR laminate sleeved actuators can be used to improve payload holding capacity for a two-digit manipulator. In future work, we will extend this concept beyond the evaluation of single actuator and evaluate the capabilities of these actuators in manipulators and human-robot interfaces.

REFERENCES

[1] K. Suzumori, "Elastic materials producing compliant robots," *Robotics and Autonomous Systems*, vol. 18, pp. 135–140, 1996.
[2] F. Ilievski, A. D. Mazzeo, R. F. Shepherd, X. Chen, and G. Whitesides, "Soft robotics for chemists," *Angewandte Chemie*, vol. 123, pp. 1930–1935, 2011.
[3] R. F. Shepherd, F. Ilievski, W. Choi, S. Morin, A. Stokes, A. D. Mazzeo, X. Chen, W. Wang, and G. Whitesides, "Multigait soft robot," *PNAS*, pp. 1–4, 2011.
[4] T. Noritsugu, M. Takaiwa, and D. Sasaki, "power assist wear driven with pneumatic rubber artificial muscles," *Int. Conference on Mechatronics and Machine Vision in Practice*, pp. 539–544, 2008.
[5] H. Schulte, "The characteristics of the mckibben artificial muscle," *The Application of External Power in Prosthetics and Orthotics*, pp. 94–115, 1961.
[6] J. Baer, "Material handling apparatus and the like," US Patent 3343864, Sept. 26, 1967.
[7] K. Suzumori, S. Iikura, and H. Tanaka, "Development of flexible microactuator and its applications to robotic mechanisms," *IEEE Int. Conf. on Robotics and Automation*, vol. 2, pp. 1622–1627, 1991.
[8] A. A. M. Faudzi, M. R. M. Razif, I. N. A. M. Nordin, K. Suzumori, S. Wakimoto, and D. Hirooka, "Development of bending soft actuator with different braided angles," *IEEE ASME Int. Conf. Advanced Intelligent Mechatronics*, pp. 1093–1098, 2012.
[9] D. Mingcong, W. Aihui, S. Wakimoto, and T. Kawashima, "Characteristic analysis and modeling of a miniature pneumatic curling rubber actuator," *IEEE Int. Conf. Advanced Mechatronic Systems*, pp. 534–539, 2011.
[10] J. Bishop-Moser, G. Krishnan, C. Kim, and S. Kota, "Design of soft robotic actuators using fluid-filled fiber-reinforced elastomeric enclosures in parallel combinations," *IEEE Int. Conf. on Intelligent Robots and Systems*, pp. 4264–4269, 2012.
[11] R. Martinez, Fish.C.R., Chen.C., and Whitesides.G.M., "Elastomeric origami: Programmable paper-elastomer composites as pneumatic actuators," *Advanced Functional Materials*, vol. 22, pp. 1376–1384, 2012.
[12] R. Martinez, Branch.J.L., Fish.C.R., Lin.L., Suo.Z., and Whitesides.G.M., "Robotic tentacles with three-dimensional mobility based on flexible elastomers," *Advanced Materials*, vol. 25, pp. 205–212, 2013.
[13] S. Obiajulu, E. Roche, F. Pigula, and C. Walsh, "Soft pneumatic artificial muscles with low threshold pressures for a cardiac compression device," *ASME IDETC/CIE*, 2013 (accepted for publication).